



A Journal of



Accepted Article

Title: Synthesis of Molecular Dyads and Triads based upon N-Annulated Perylene Diimide Monomers and Dimers

Authors: Jonathan R. Cann, Clement Cabanetos, and Gregory Charles Welch

This manuscript has been accepted after peer review and appears as an Accepted Article online prior to editing, proofing, and formal publication of the final Version of Record (VoR). This work is currently citable by using the Digital Object Identifier (DOI) given below. The VoR will be published online in Early View as soon as possible and may be different to this Accepted Article as a result of editing. Readers should obtain the VoR from the journal website shown below when it is published to ensure accuracy of information. The authors are responsible for the content of this Accepted Article.

To be cited as: *Eur. J. Org. Chem.* 10.1002/ejoc.201801383

Link to VoR: <http://dx.doi.org/10.1002/ejoc.201801383>

Supported by



WILEY-VCH

Synthesis of Molecular Dyads and Triads based upon N-Annulated Perylene Diimide Monomers and Dimers

Mr. Jonathan R. Cann,¹ Dr. Clement Cabanetos,² Prof. Gregory C. Welch^{1*}

¹Department of Chemistry, University of Calgary, 2500 University Drive N.W., Calgary, Alberta, T2N 1N4, Canada.

²CNRS UMR 6200, MOLTECH-Anjou, University of Angers, 2 Bd Lavoisier, Angers, France, 49045

*E-mail: gregory.welch@ucalgary.ca

*Webpage: <http://welchlab.wixsite.com/website>

KEYWORDS: Organic Dyes, Perylene Diimide, N-Annulation, Phenothiazine, Molecular Dyads and Triads

ABSTRACT: The synthesis of N-annulated perylene diimides (NPDI) with grafted electron donating phenothiazine (PTZ) groups is presented. The synthetic strategy takes advantage of the N-annulation at the PDI bay position which allows for the facile installation of the pendant donors. Three new molecular materials are reported, a dyad consisting of an NPDI monomer tethered to a PZT unit (**4**), a dyad consisting of an NPDI dimer with one PZT unit tethered (**9**), and a triad consisting of an NPDI dimer with two PTZ units tethered (**10**). The PTZ and NPDI were ‘clicked’ together using copper catalyzed alkyne-azide cycloaddition chemistry. Analysis of optical absorption/emission spectra and electrochemical data reveal that the electronic structure of each individual aromatic system remains distinct, but through-space interactions occurs as evident by fluorescence quenching in both solution and the solid-state.

1. Introduction

Organic molecular and polymeric dyads and triads are systems where two or more distinct π -conjugated systems are present in the same material. Such dyads and triads have been explored for many applications ranging from fundamental energy^[1] or charge transfer studies^[2,3] to functional applications like fluorescence sensing,^[4] ambipolar organic field effect transistors^[5,6] and single component organic photovoltaics.^[7–11] Dyad systems are built having well-defined electron donor and acceptor components, which have an energetic offset in their frontier molecular orbitals enabling charge transfer, energy transfer, or both hole and electron transport. These systems can be designed either with metal-ligand complexes, which are especially effective for photocatalytic transformations,^[12] or with organic π -conjugated systems which have found a wide variety of uses in opto-electronic applications.^[13]

One building block that is popular for use as the acceptor portion of organic dyads and triads is the perylene diimide (PDI) chromophore. PDI has been thoroughly studied in many optoelectronic applications owing to its commercial availability, high thermal stability, low lying frontier molecular orbitals, high visible light absorption, and synthetic versatility.^[14–18] PDI-based dyads have been used in a wide variety of applications including studies on Forster resonance energy transfer,^[19] charge transfer,^[20–23] water photooxidation,^[24] fluorescence sensors,^[25] molecular logic operations,^[26] and single component organic photovoltaics.^[27,28] In the majority of these systems, the donor unit is tethered to the PDI through the imide position via an alkyl,^[21,25,29–31] aryl,^[23,24,27,28,32] or no linker^[19,20] owing to ease of installing amine functionalized compounds at the imide positions. There are only a few examples of PDI based dyads being tethered at bay positions, either via alkoxy^[26,33] or N-annulated^[34] linkers.

Owing to the many possible applications for these types of PDI materials, a more versatile method toward the underexplored bay tethered dyads is attractive to expand the scope of donors that can be tethered to the PDI. A wider scope of bay-tethered PDI dyads would facilitate the exploration of the differences in the electronic and physical properties between imide and bay linked dyads.

In this contribution we detail a synthetic pathway towards bay functionalized PDI based molecular dyads. Our synthetic strategy centers on the functionalization of the PDI at the bay position via N-annulation.^[35–41] Three target materials are shown in Figure 1. The first target is the dyad **4** (**NPDI_{hex}PTZ**) based on a monomeric N-annulated PDI acceptor, tethered via a hexyl chain and triazole ring to a phenothiazine donor. Each portion of this molecule was carefully chosen for this system. The N-annulation at the bay position of the PDI chromophore is unique as it enables alkyl chain substitution at a position other than the imides, allows free choice of imide side chains to influence solubility and self-assembly, renders the PDI core prone to reversible oxidation, and tethers the donor at the short axis of PDI (as opposed to the long axis when tethering via the imide) will provide different supramolecular organization. The hexyl chain is a long, non-conjugated, aliphatic linker that introduces flexibility between the donor and acceptor components. The triazole unit, a result of utilizing copper catalyzed alkyne-azide cycloaddition (click) chemistry for the rapid generation of the target materials, has been shown previously to be outside the redox window of PDI-donor dyad systems.^[31] Finally, phenothiazine was chosen as the donor because it is electron rich relative to PDI and is known to form stable radical cations, enabling a long-lived charged state which, has been utilized in dye sensitized solar cells and redox flow batteries, thus serving as a good model donor.^[42–44]

This molecular design was further extended to dyad and triad systems based on a dimeric N-annulated perylene diimide (**NPDI_{hex2}**) acceptor. Dimeric PDI based materials have been frequently used in high performance non-fullerene electron acceptors in organic solar cells,^[36,45,46] but have yet to be fully exploited in dyad/triad type systems with only one system reported to date.^[34] The dyad **9** (**NPDI_{hex2}PTZ**) and triad **10** (**NPDI_{hex2}PTZ₂**) were targeted and contain a dimeric NPDI based acceptor with one and two PTZ units, respectively, extending out from the N-annulated bay position.

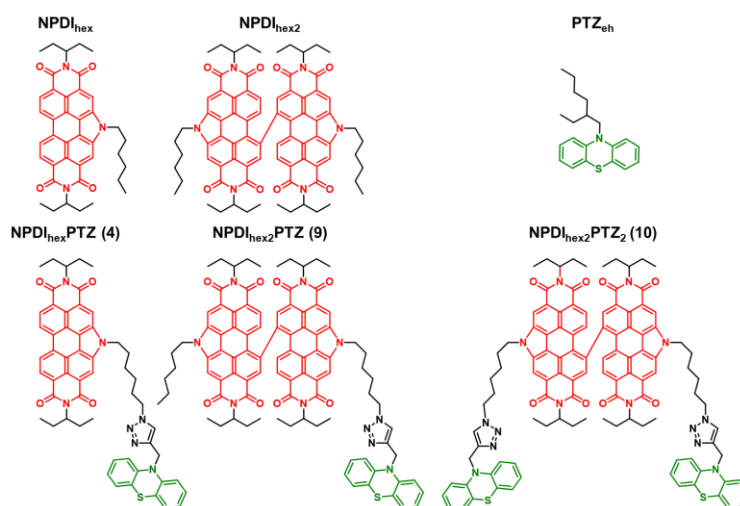


Figure 1: Top) Reference NPDI monomer **NPDI_{hex}**, dimer **NPDI_{hex2}**, and PTZ reference **PTZ_{eh}**. Bottom) Target monomer-based dyad **4** (**NPDI_{hex}PTZ**), dimer-based dyad **9** (**NPDI_{hex2}PTZ**), and dimer-based triad **10** (**NPDI_{hex2}PTZ₂**).

2. Results and Discussion

2.1 Synthesis:

To synthesize **4** (**NPDI_{hex}PTZ**) from previously synthesized **1** (**NHPDI**),^[36] three reactions must occur: alkylation of **1** (**NHPDI**) with a doubly functionalized alkyl chain, azide formation on one end of the alkyl chain, and click between the azide functionalized alkyl chain and the acetylene functionalized donor PTZ. The alkylation was performed before the azide was introduced to the alkyl chain to avoid the synthesis of a potentially hazardous lightweight alkyl-azide. This route

leaves the click reaction for the last step which increases the synthetic versatility when exploring alternative donor components.

There are at least two extra steps involved in the synthesis of dyads/triads based on dimeric NPDI₂: bromination at one of the remaining bay positions of the NPDI and aryl-aryl coupling. While brominating **4** (NPDI_{hex}PTZ) would be ideal, it was ultimately unfeasible due to undesired reactivity at the triazole and phenothiazine. Instead it was necessary to brominate a step earlier to transform **3** (NPDI_{hex}N₃) to **5** (Br-NPDI_{hex}N₃) which was then clicked onto the donor and coupled either asymmetrically or symmetrically to give the NPDI dimer based dyad and triad **9** (NPDI_{hex2}-PTZ) and **10** (NPDI_{hex2}PTZ₂), respectively.

The first target was the monomeric NPDI dyad, **4** (NPDI_{hex}PTZ), which was synthesized in three steps from **1** (NHPDI) (Figure 2).^[36] First, **1** (NHPDI) was alkylated with a large excess of 1,6-dibromohexane thereby preventing the formation of an alkyl-linked dimer. Using standard N-H alkylation conditions^[36] with temperatures of 120 °C, the target product, **2** (PDI_{hex}Br), was formed, but a significant amount of alkene terminated side-product, a result of Br-elimination, was observed and proved difficult to separate. Lowering the temperature from 120 °C to 60 °C prevented the formation of the alkene side-product and gave **2** (PDI_{hex}Br) in yields of 70%.

The reaction of compound **2** (NPDI_{hex}Br) with excess NaN₃ yielded the azide functionalized compound **3** (NPDI_{hex}N₃) in yields up to 95%. The click reaction of **3** (NPDI_{hex}N₃) with the alkyne functionalized donor PTZac (which was synthesized according to literature procedure, see Figure 2)^[47] resulted in the formation of the first targeted dyad, **4** (NPDI_{hex}PTZ) with 80% yield. Overall, **4** (NPDI_{hex}PTZ) can be synthesized in 6 steps from commercially available starting materials with a overall yield of 33% yield based on the perylene tetracarboxylic dianhydride starting material.^[36] The closely related, and only previously reported, NPDI dyad can

be synthesized in only 4 steps, but with a much lower overall yield of ~5-10% depending on the donor.^[34] Therefore, the route presented here offers the significant advantage of a higher overall yield.

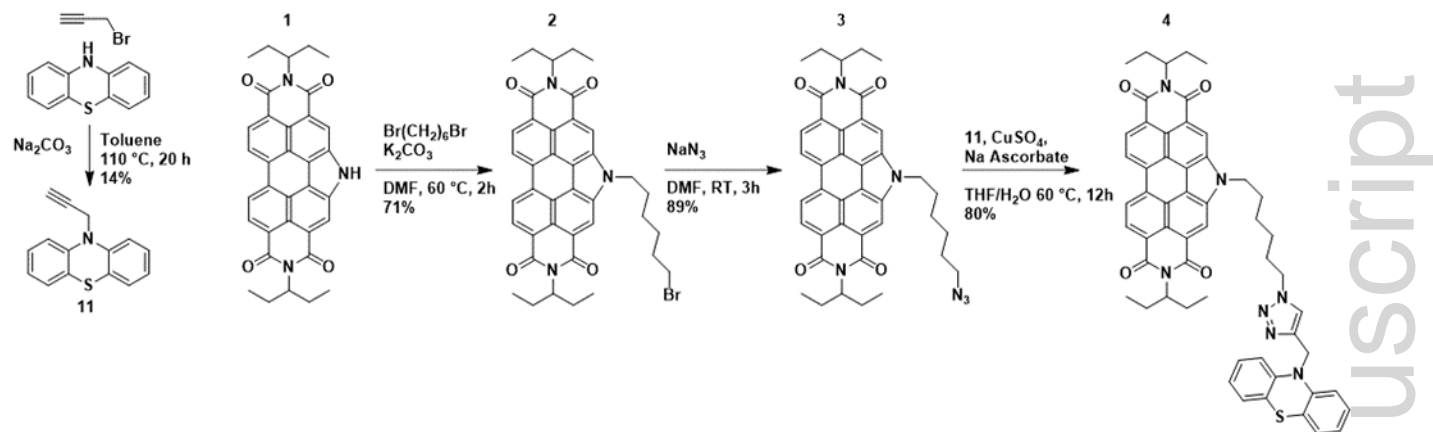


Figure 2: Synthetic route towards the donor precursor **11** (PTZ_{ac}) and the monomeric NPDI dyad **4** (NPDI_{hex}PTZ).

The second target was the dimeric NPDI dyad, **9** (NPDI_{hex2}PTZ), which requires an aryl-aryl coupling reaction to form the dimeric NPDI. Our procedure involved the near quantitative bromination of compound **3** (NPDI_{hex}N₃) to give compound **5** (BrNPDI_{hex}N₃). Compound **5** (BrNPDI_{hex}N₃) was then clicked with the alkyne functionalized **11** (PTZ_{ac}) to give **6** (BrNPDI_{hex}PTZ) in yields above 70%. To synthesize the target dyad, a coupling partner with a transmetalating agent had to be synthesized. The two most common transmetalating groups are boronic esters and trialkyl-tin groups for Suzuki and Stille reactions, respectively, and both are known for PDI based materials.^[48,49] While the borylation of PDI is known, borylations were unable to be replicated on NPDI_{hex}. Therefore, a Stille coupling reaction was utilized. Compound **7** (BrNPDI_{hex}) was stannylated with hexabutyltin utilizing the catalyst SiliaCat[®] DPP-Pd to give **8** (Bu₃SnNPDI_{hex}) in 63% yield (Figure 3). An identified by-product was the dimer NPDI_{hex2} (Figure 1) which forms because of ligand redistribution during the catalytic cycle. The target dimeric PDI dyad **9** (NPDI_{hex2}PTZ) was successfully synthesized and isolated in 45% after

column chromatography via the Stille cross-coupling reaction between **6** (**BrNPDI_{hex}PTZ**) and **8** (**Bu₃SnNPDI_{hex}**) (Figure 3). Column chromatography is required to separate product **9** (**NPDI_{hex2}PTZ**) from **4** (**NPDI_{hex}PTZ**) which is produced as a minor side product.

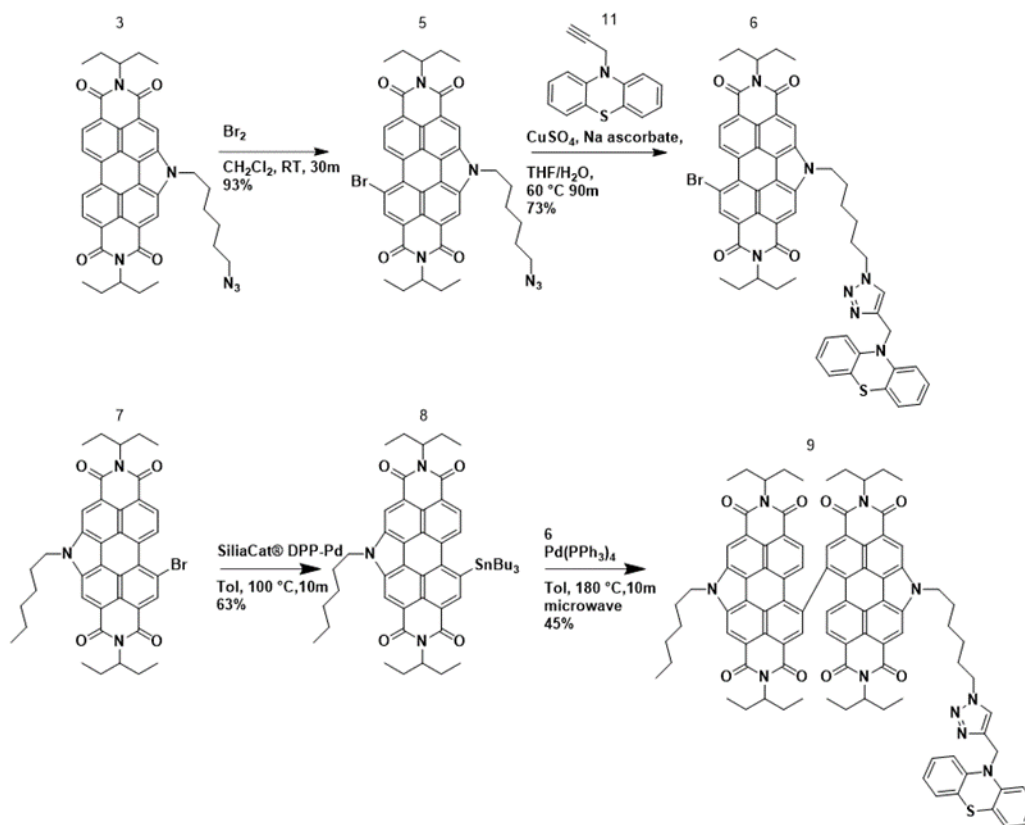


Figure 3 Synthetic route toward dimeric NPDI_{hex} dyad **9** (**NPDI_{hex2}PTZ**) via Stille reaction.

To explore an alternative route that avoided the use of organotin reagents, **9** (**NPDI_{hex2}PTZ**) was synthesized via an asymmetric coupling based on our previously optimized modified Negishi reaction (Figure 4).^[36] The coupling of **6** (**BrNPDI_{hex}PTZ**) and **7** (**BrNPDI_{hex}**) gave the target dimer **9** (**NPDI_{hex2}PTZ**) in 38% yield. Considering the similar electronics of the aryl-Br bonds it is unsurprising that the symmetric dimers **NPDI_{hex2}** and **10** (**NPDI_{hex2}PTZ₂**) were also formed in 16% and 24% yield, respectively (78% total recovery). All compounds could be separated from one another using silica-gel column chromatography.

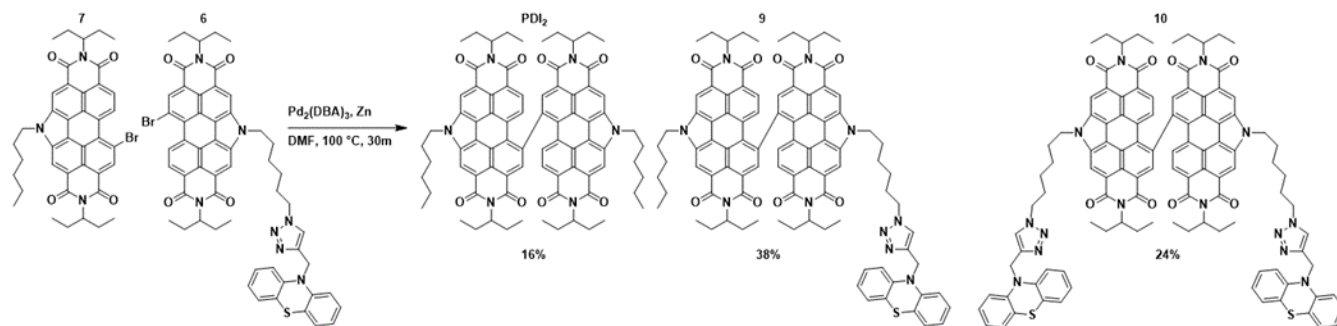


Figure 5: Synthetic route toward dimeric NPDI dyad **9** ($\text{NPDI}_{\text{hex}2}\text{PTZ}$) via Negishi reaction.

The final target was the dimeric NPDI triad, **10** ($\text{NPDI}_{\text{hex}2}\text{PTZ}_2$). The direct synthesis was easily achieved through the dimerization of **6** ($\text{BrNPDI}_{\text{hex}}\text{PTZ}$) via using the modified Negishi-type homocoupling with a 66% yield (Figure 5).

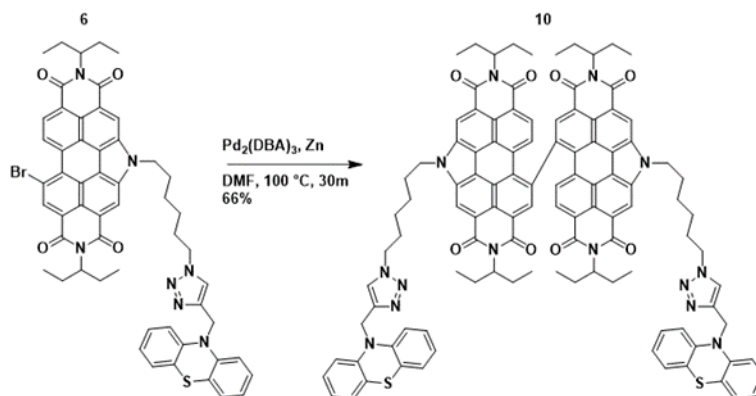


Figure 4: Synthetic route toward dimeric NPDI dyad **10** ($\text{NPDI}_{\text{hex}2}\text{PTZ}_2$) via Negishi reaction.

The three targets compounds **4** ($\text{NPDI}_{\text{hex}}\text{PTZ}$), **9** ($\text{NPDI}_{\text{hex}2}\text{PTZ}$), and **10** ($\text{NPDI}_{\text{hex}2}\text{PTZ}_2$) were identified by ^1H and ^{13}C NMR spectroscopy, MALDI-TOF mass spectrometry, and elemental analysis. Full spectra and analysis reports are provided in the supporting information.

2.2 NMR Spectroscopic Analysis

The chemical shifts of aromatic proton resonances of the PDI chromophore have been shown to be very sensitive to the steric electronic environment.^[50–52] For this reason the aromatic region of the ^1H NMR spectra of NPDI_{hex} , **4** ($\text{NPDI}_{\text{hex}}\text{PTZ}$), **9** ($\text{NPDI}_{\text{hex}2}\text{PTZ}$), **10** ($\text{NPDI}_{\text{hex}2}\text{PTZ}_2$), and $\text{NPDI}_{\text{hex}2}$ were compared (Figure 6). The ^1H NMR spectrum of **4**

(**NPDI_{hex}PTZ**) (Figure 6 – Red) shows two groups of aromatic proton resonances. The first set of proton resonances is from 6.5 to 7.5 ppm attributed to the phenothiazine and triazole protons (ca. 7.2 ppm). The second set of resonances above 7.5 ppm are attributed to the PDI protons (as confirmed by comparing to **NPDI_{hex}**, see Figure 6 - Black). When comparing the spectra of **4** (**NPDI_{hex}PTZ**) (Figure 6 – Red) and **NPDI_{hex}** (Figure 6 – Black) there are only slight shifts of the PDI based protons.

Comparing monomeric dyad **4** (**NPDI_{hex}PTZ**) (Figure 6 – Red) to the dimeric dyad **9** (**NPDI_{hex2}PTZ**) (Figure 6 – Blue) there are several distinct differences. First, the NPDI peaks separate into 7 peaks consisting of 4 singlets, each integrating for one proton; two broad singlets, each integrating for two protons, and a doublet of doublets integrating for 2 protons. The splitting pattern here is reminiscent of the reference donor **NPDI_{hex2}** (Figure 2 – Purple) which consists of

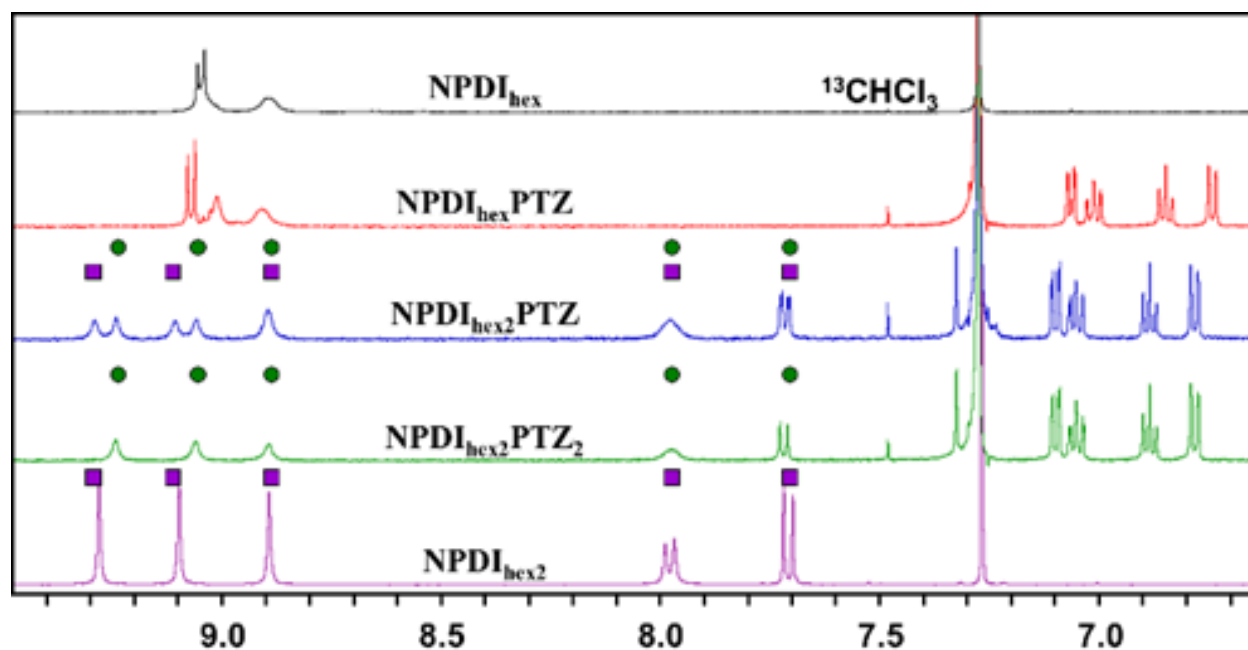


Figure 6: Stacked ¹H NMR spectra of **NPDI_{hex}** (black), **4** (**NPDI_{hex}PTZ**, red), **9** (**NPDI_{hex2}PTZ**, blue), **10** (**NPDI_{hex2}PTZ₂**, green), and **NPDI_{hex2}** (purple) in CDCl₃. Peaks that correlate well between **9** (**NPDI_{hex2}PTZ**, blue) and **10** (**NPDI_{hex2}PTZ₂**, green), are indicated with green circles and Peaks that correlate well between **9** (**NPDI_{hex2}PTZ**, blue) and **NPDI_{hex2}** (purple), are indicated with purple squares.

three singlets and two doublets; each of which corresponds perfectly with a peak in **9** (**NPDI_{hex2}PTZ**) (marked with purple squares). Resonances at 6.5-7.3 ppm in the spectrum of **9** (**NPDI_{hex2}PTZ**) are attributed to the PTZ donor group. Unexpectedly the PTZ peaks in **9** (**NPDI_{hex2}PTZ**) do not correspond exactly with the PTZ peaks in **4** (**NPDI_{hex}PTZ**) which may indicate some NPDI – PTZ interaction in **4** (**NPDI_{hex}PTZ**) which is disrupted by the dimerization of the NPDI in **9** (**NPDI_{hex2}PTZ**).

Finally, looking at **10** (**NPDI_{hex2}PTZ₂**) (Figure 2 – Green) the NPDI based protons have coalesced to 3 singlets and two doublets, similar to **NPDI_{hex2}**, but each slightly shifted. The shifted NPDI peaks are likely due to the interaction with the tethered PTZ as discussed above. Comparing **9** (**NPDI_{hex2}PTZ**) to **10** (**NPDI_{hex2}PTZ₂**), it is evident that the peaks in **9** (**NPDI_{hex2}PTZ**) that do not correspond to **NPDI_{hex2}** correspond directly with **10** (**NPDI_{hex2}PTZ₂**) (marked with green circles). Thus, the nature of the side-chain at the pyrrolic N-position has a slight impact on the electronics of the NPDI core.

Based on the shifts of both the characteristic NPDI and PTZ resonances in the materials studied, the chromophores have some interaction with each other in the solution phase, but the nature of the interaction is dependent on whether the NPDI core is monomeric or dimeric.

2.3 Electrochemical Properties:

The electrochemical properties of **4** (**NPDI_{hex}PTZ**), **9** (**NPDI_{hex2}PTZ**), **10** (**NPDI_{hex2}PTZ₂**) were examined using cyclic voltammetry (see Figure 7 and Table 1, full analysis can be found in the supporting information Figure S28). First, looking at **4** (**NPDI_{hex}PTZ**) and comparing to the reference compounds **NPDI_{hex}** and **PTZ_{eh}** (see Figure 7A), **4** (**NPDI_{hex}PTZ**) has two fully reversible reduction events and two partially reversible oxidation events. Both reduction

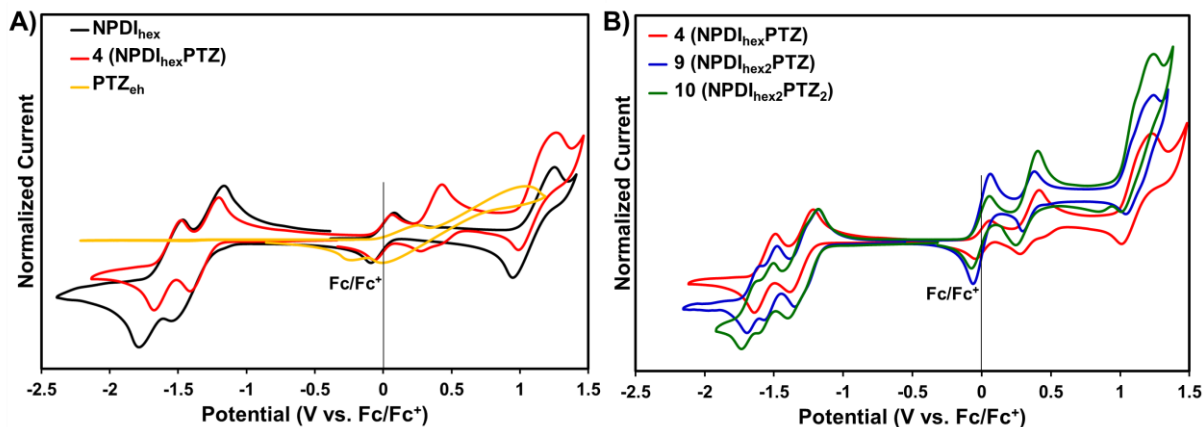


Figure 7: A) Stacked cyclic voltammetry plot of **4** (**NPDI_{hex}PTZ**, red), compared to reference compounds **PDI** (black) and **PTZ** (yellow). B) Stacked cyclic voltammetry plot of **4** (**PDI-PTZ**, red), **9** (**NPDI_{hex2}PTZ**, blue), and **10** (**NPDI_{hex2}PTZ₂**, green). Each trace has been individually referenced to ferrocene, and current intensity has been normalized to the first reverse reduction peak.

waves line up with the reference compound **NPDI_{hex}** and are assigned to isolated one electron reductions within the PDI core, which has previously shown to undergo two fully reversible reductions.^[17,36] The first of the two oxidation events ($E_{1/2}$ 0.34 V vs. Fc/Fc^+) correlates with the oxidation of **PTZ_{eh}**, and the second oxidation ($E_{1/2}$ 1.13 V vs. Fc/Fc^+) correlates with the oxidation of **NPDI_{hex}**. The close correlation between **4** (**NPDI_{hex}PTZ**) and the individual reference compounds indicates that the triazole is not redox active in the region of interest, and that the **NPDI_{hex}** and **PTZ_{eh}** subunits are not in direct electronic communication.

Comparing the CV traces of **4** (**NPDI_{hex}PTZ**), **9** (**NPDI_{hex2}PTZ**), and **10** (**NPDI_{hex2}PTZ₂**) there are three major changes (see Figure 7B). Looking at the reduction waves, there are two reversible reductions for **4** (**NPDI_{hex}PTZ**) but four reversible reductions each for **9** (**NPDI_{hex2}PTZ**) and **10** (**NPDI_{hex2}PTZ₂**). The additional reduction waves are due to dimerized PDI core since each individual PDI has two distinct reductions. The $E_{1/2}$ of the first reduction occurs at -1.30 V for **4** (**NPDI_{hex}PTZ**) and -1.21 V for **9** (**NPDI_{hex2}PTZ**) and -1.24 for **10**

(**NPDI_{hex2}PTZ₂**). The slight lowering of the reduction potential is a result of the dimerization of the PDI core and has been observed previously.^[36]

Compounds **4** (**NPDI_{hex}PTZ**), **9** (**NPDI_{hex2}PTZ**), and **10** (**NPDI_{hex2}PTZ₂**) all have two partially reversible oxidations: one with $E_{1/2}$ at ~ 0.32 V corresponding to oxidation of the PTZ donor, and one with $E_{1/2}$ at ~ 1.15 V which corresponds to the oxidation of the N-annulated PDI. Importantly, the only major difference between the three compounds is the intensity of the oxidation peak at ~ 0.32 V, which correlates to the different ratios of PDI to PTZ in each compound. All oxidation waves occur at the same potential across all three compounds, indicating that the oxidations are insensitive to the structural modifications and that the electronic communication is minimal between the donor and acceptor chromophores.

Table 1: Tabulated electrochemical data for **NPDI_{hex}**, **4** (**NPDI_{hex}PTZ**), **9** (**NPDI_{hex2}PTZ**), **10** (**NPDI_{hex2}PTZ₂**), and **NPDI_{hex2}**. See SI Figure S28 for full analysis of CV traces.

	Red _{onset}	EA	$E_{1/2}$ Red	Ox _{onset}	IP	$E_{1/2}$ Ox
NPDI_{hex} ³⁶	-1.30	3.5	N/A	0.90	5.7	N/A
4 (NPDI_{hex}PTZ)	-1.13	3.7	-1.30, -1.55	0.24	5.0	0.34, 1.13
9 (NPDI_{hex2}PTZ)	-1.06	3.7	-1.21, -1.31, -1.55, -1.63	0.26	5.1	0.32, 1.15
10 (NPDI_{hex2}PTZ₂)	-1.08	3.7	-1.24, -1.34, -1.55, -1.68	0.23	5.0	0.32, 1.13
NPDI_{hex2} ³⁶	-1.04	3.8	-1.24, -1.35, -1.53, -1.66 ⁴¹	1.2	6.0	N/A

Electron affinity (EA) = $4.8 + E(\text{Red}_{\text{onset}})$. Ionization Potential (IP) = $4.8 + E(\text{Ox}_{\text{onset}})$. See SI Materials and Methods and Figure S29 for onset determination.

2.4 Optical properties:

UV-Vis Absorption

The optical absorption spectrum of **4** ($\text{NPDI}_{\text{hex}}\text{PTZ}$) in solution is shown in Figure 8A. The optical profile is dominated by strong absorption from 400 nm to 550 nm which is similar in intensity and profile to that of NPDI_{hex} and is typical of PDI based materials.^[17] There is a small increase in the absorption band in the high energy region of **4** ($\text{NPDI}_{\text{hex}}\text{PTZ}$) relative to NPDI_{hex} (300-350 nm, see Figure 3A) which is attributed to localized transitions in the PTZ unit.

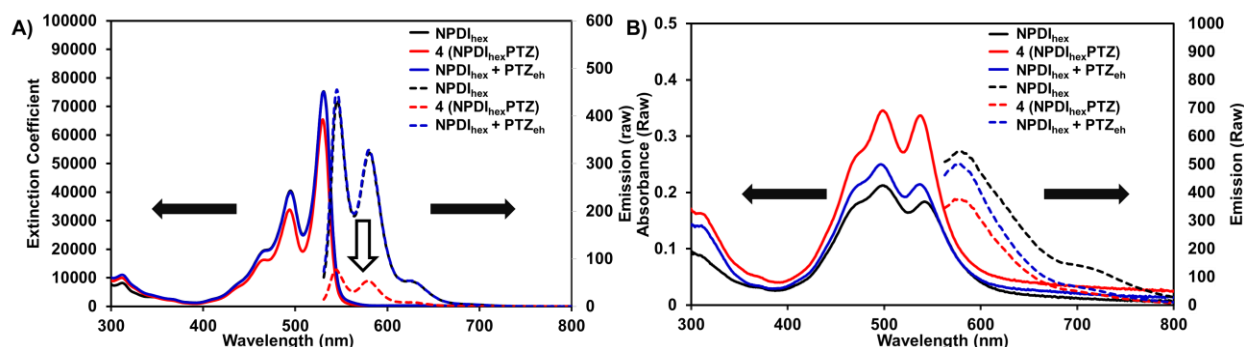


Figure 8: Solution UV-Vis (solid lines) and photoluminescence (dashed lines) spectra of **4** ($\text{NPDI}_{\text{hex}}\text{PTZ}$, red) as well as reference compound NPDI_{hex} with 0 (black) or 1 (blue) equivalent of PTZ_{eh} . **B)** Thin film UV-Vis (solid lines) and photoluminescence (dashed lines) spectra of **4** ($\text{NPDI}_{\text{hex}}\text{PTZ}$, red) as well as reference compound NPDI_{hex} with 0 (black) or 1 (blue) equivalent of PTZ_{eh} . NPDI_{hex} was cast from 10 mg/mL solutions in chloroform on glass at 1500 RPM for 30 s. All other films were equimolar and cast from the same conditions as NPDI_{hex} .

The optical absorption spectrum of **4** ($\text{NPDI}_{\text{hex}}\text{PTZ}$) in thin film is shown in Figure 8B. As in solution, the profile is dominated by the PDI absorption from 450 nm to 600 nm. Relative to the solution profiles the main absorption band is broadened, the onset red shifted from 539 nm to 563 nm and the λ_{max} moves from the lowest energy peak at 538 nm (0-0 vibronic transition), to the next lowest energy peak at 500 nm (0-1 vibronic transition). Both the bathochromic shift and increase in relative intensity of the 0-1 peak is attributed to π -stacking of the PDI chromophores, which is expected when transitioning from solution to thin film absorptions.^[53,54]

Unlike the solution profile, there are several major differences between the profiles of **4** ($\text{NPDI}_{\text{hex}}\text{PTZ}$) and neat NPDI_{hex} . First, the intensity is increased across the entire window which likely indicates a thicker film. Second, the profile of the trace is markedly different; for NPDI_{hex}

the 0-0 peak (538 nm) is considerably less intense than the 0-1 peak (496 nm), but for **4** (**NPDI_{hex}PTZ**) the 0-0 peak is nearly equal to the 0-1 peak. The reduced relative intensity of the 0-0 peak indicates less PDI π -stacking which is likely due to the steric hindrance of the tethered phenothiazine.

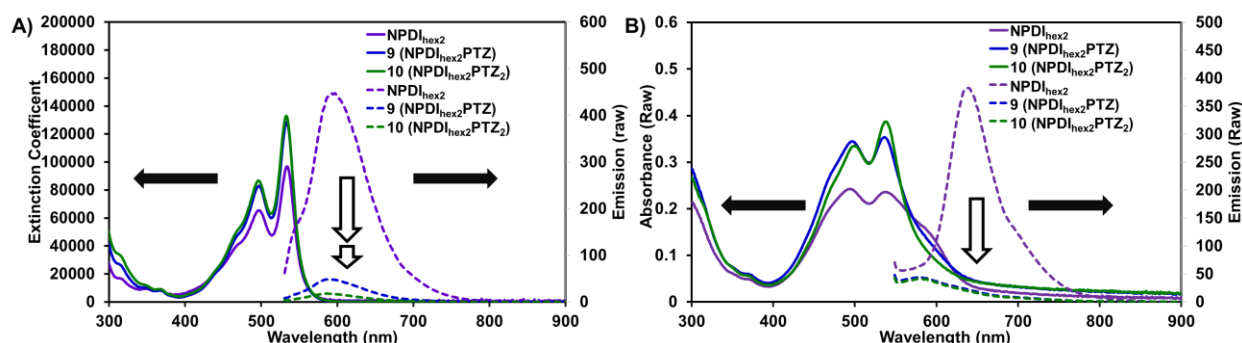


Figure 9: Solution UV-Vis (solid lines) and photoluminescence (dashed lines) spectra of **NPDI_{hex2}**, **9** (**NPDI_{hex2}PTZ**), and **10** (**NPDI_{hex2}PTZ₂**). **B)** Thin film UV-Vis (solid lines) and photoluminescence (dashed lines) spectra **NPDI_{hex2}**, **9** (**NPDI_{hex2}PTZ**), and **10** (**NPDI_{hex2}PTZ₂**). Films of **NPDI_{hex2}** were cast from 10 mg/mL solutions in chloroform on glass at 1500 RPM for 30 s. Other solutions were equimolar and cast from the same conditions as **NPDI_{hex2}**.

The optical absorption profiles of **9** (**NPDI_{hex2}PTZ**) and **10** (**NPDI_{hex2}PTZ₂**) in solution are shown in Figure 9A. Both profiles are dominated by the PDI absorption from 450-550 nm, and both have an absorption band from 300-350 nm which is partially due to the phenothiazine. As expected **9** (**NPDI_{hex2}PTZ**) and **10** (**NPDI_{hex2}PTZ₂**) have nearly identical absorption profiles except that the intensity of **9** (**NPDI_{hex2}PTZ**) from 300 nm to 350 nm is slightly lower than that of **10** (**NPDI_{hex2}PTZ₂**) due to the additional PTZ unit on **10** (**NPDI_{hex2}PTZ₂**).

The optical absorption spectrum of **9** (**NPDI_{hex2}PTZ**) and **10** (**NPDI_{hex2}PTZ₂**) in thin films is shown in Figure 9B. In solution, the profile is dominated by the **NPDI_{hex2}** absorption from 450 nm to 625 nm. Relative to the solution profiles the main absorption band is broadened and the onset of absorption red shifted from 545 nm to 551 nm. As depicted, above, the broadened, redshifted absorption band indicates some extent of π -stacking in the solid state.

Comparing to the reference compound **NPDI_{hex2}** there are some key differences in the thin film absorption profiles. First, the overall intensity is higher which likely indicates a thicker film. Second, in the thin film profile of **NPDI_{hex2}** there is a shoulder at ~600 nm, but this shoulder is smaller in **9 (NPDI_{hex2}PTZ)** and is completely absent in **10 (NPDI_{hex2}PTZ₂)**. Additionally, in **NPDI_{hex2}**, the 0-0 peak at 540 nm is less intense than the 0-1 peak at 497 nm, but in **9 (NPDI_{hex2}PTZ)** the 0-0 peak (530 nm) is slightly more intense than the 0-1 peak (499 nm), and in **10 (NPDI_{hex2}PTZ₂)** the 0-0 peak (539 nm) is considerably more intense than the 0-1 peak (501 nm). The relative intensity of the 0-0 and 0-1 peaks as well as the significant low energy shoulder indicates that **NPDI_{hex2}** exhibits a strong tendency to aggregate in the solid-state,^[55] but **9 (NPDI_{hex2}PTZ)** and **10 (NPDI_{hex2}PTZ₂)** have inhibited aggregation indicating that each additional phenothiazine might be preventing the NPDI dimers from forming organized supramolecular structures.

Photoluminescence

To further probe the potential interaction between the donor and acceptor chromophores we examined the solution and thin film light emission characteristics. The photoluminescence (PL) spectra of compounds **4 (NPDI_{hex}PTZ)**, **9 (NPDI_{hex2}PTZ)**, and **10 (NPDI_{hex2}PTZ₂)** and a model system containing equimolar amounts of non-tethered chromophores are shown in Figures 8 and 9.

Comparing the solution PL spectrum of **4 (NPDI_{hex}PTZ)** to the PL spectra of either neat **NPDI_{hex}**, or the model system **NPDI_{hex} + PTZ_{eh}** in solution, the emission of the tethered system **4 (NPDI_{hex}PTZ)** is reduced by 83% (See Figure 8A, Table 2). Since PDI absorbs lower energy than PTZ, the fluorescence quenching is not a result of Forster resonance energy transfer but rather is a

result of a charge transfer between the donor and acceptor chromophores. Since the PL quenching is only observed in **4** (**NPDI_{hex}PTZ**) and not in the equimolar model system, the charge transfer must be dependent on both the presence and proximity of the donor component.

Comparing the thin film PL spectrum of **4** (**NPDI_{hex}PTZ**) to the PL spectra of either neat **NPDI_{hex}**, or the model system **NPDI_{hex} + PTZ_{eh}** in thin film, the emission of the tethered system **4** (**NPDI_{hex}PTZ**) is reduced by 31% and the blend system is reduced by 10% (See Figure 8B, Table 2). This quenching indicates that in the solid state the **PTZ** donor can quench the emission of **NPDI_{hex}**. However, in the blended films (**NPDI_{hex} + PTZ_{eh}**) the PL quenching efficiency is less than that of films of the tethered system **4** (**NPDI_{hex}PTZ**). This indicates that phase separation occurs between **NPDI_{hex}** and **PTZ_{eh}** in the solid state and highlights the uniqueness of the tethered system

When comparing the PL spectra of **9** (**NPDI_{hex2}PTZ**) and **10** (**NPDI_{hex2}PTZ₂**) to **NPDI_{hex2}**, the emission of **9** (**NPDI_{hex2}PTZ**) is quenched by 89% and **10** (**NPDI_{hex2}PTZ₂**) is quenched by 96%. This is consistent with the increasing number of **PTZ** units (See Figure 4). The non-tethered models show no PL quenching in solution (See SI Figure S28).

As thin films, nearly complete PL quenching is observed for both **9** (NPDI_{hex2}PTZ) and **10** (NPDI_{hex2}PTZ₂) (see Figure 9), and for both blended systems (See Figure S29). The high PL quenching in all cases indicates that like the monomeric NPDI_{hex} based materials, PTZ does quench the emission from NPDI_{hex}. Unlike NPDI_{hex}, NPDI_{hex2} is miscible with PTZ_{eh} and therefore minimal phase separation is observed, and the PL quenching is high in both tethered and blended films.

Table 2: Tabulated spectral data for **4** (NPDI_{hex}PTZ), **9** (NPDI_{hex2}PTZ), and **10** (NPDI_{hex2}PTZ₂).

	State	λ_{\max} (nm)	ϵ (L/mol*cm)	λ_{onset} (nm)	PL λ_{\max} (nm)	Quenching %
4 (NPDI _{hex} PTZ)	Sln	530	65 500	539	545	83 %
	Film	500	N/A	563	581	31 %
9 (NPDI _{hex2} PTZ)	Sln	533	128 600	545	590	89 %
	Film	530	N/A	551	579	88 %
10 (NPDI _{hex2} PTZ ₂)	Sln	533	132 800	545	590	96 %
	Film	539	N/A	551	581	90 %

3. Conclusion:

We have successfully developed new synthetic methods towards PDI based molecular dyads and triads. Our strategy involves using an N-annulated PDI for which donor components are tethered via the pyrrolic N-atom position.

As a proof of concept, three materials were synthesized, one dyad based on a monomeric NPDI as well as a dyad and triad each based on an NPDI dimer. A close examination of the ¹H NMR spectra showed that there is only minimal solution-state interaction between the PDI acceptor and PTZ donor. Additionally, this interaction is altered by the steric environment around

the PDI. Further characterization by CV indicates that the frontier orbitals of the donor and acceptor are independent from each other. Similarly, the UV-Vis spectra showed that the absorption profile is well-modelled by a linear combination of the donor and acceptor units which further indicates minimal electronic communication between the chromophores. An important difference is visible in the fluorescence spectra where the dyads and triads exhibit significant PL quenching.

Finally, this work provides a facile method for the synthesis of donor-acceptor systems based on NPDI monomers and dimers where the aromatic systems are not in direct electronic communication may serve as useful materials for ambipolar OFETS and single component OPVs.

4. EXPERIMENTAL

PTZ_{ac} (11): To a 10-20 mL microwave vial with a stir bar was added Phenothiazine (1000 mg, 5 mmol), sodium carbonate (835 mg, 7.5 mmol) and toluene (10 ml). The vial was capped and purged with N₂ for 15 minutes. To the reaction mixture was added propargyl bromide (2.3 mL, 2.9 g, 25 mmol). The solution was heated to 110 °C in a bead bath with stirring. After 20 h the reaction was extracted with 1 M HCl in water. The organic phase was dried with brine. The solvent was removed on a rotatory evaporator and the solid was filtered from methanol. The solid was purified by column chromatography (hexanes → 50% CH₂Cl₂ in hexanes) to give crude **PTZ_{ac}**. Crude **11** was additionally purified via recrystallization from methanol to further to give **PTZ_{ac}** (171 mg, 14%) as a white crystalline solid. **¹H NMR:** (500 MHz, CDCl₃) δ 7.20 (dtd, *J* = 9.5, 8.1, 1.4 Hz, 4H, aryl), 7.14 (dd, *J* = 7.6, 1.3 Hz, 2H, aryl), 6.96 (td, *J* = 7.4, 1.4 Hz, 2H, aryl), 4.53 (d, *J* = 2.4 Hz, 2H, methylene), 2.46 (t, *J* = 2.4 Hz, 1H, alkynyl).

NPDI_{hex}Br (2): To a 10-20 mL microwave vial with a stir bar was added **NHPDI** (500 mg, 0.92 mmol) and potassium carbonate (253 mg, 1.8 mmol). The vial was capped and 7 mL DMF was added. The vial was purged with N₂ for 15 min. To the vial was added 1,6-dibromohexane (0.7

mL, 1.1g, 4.6 mmol). The reaction mixture was heated in a bead bath at 60 °C for 2 h. After TLC indicated the starting material had been completely consumed, the reaction mixture was diluted with 50 mL MeOH and filtered. The collected solid was washed multiple times with water and methanol to remove residual carbonates and 1,6-dibromohexane. The red solid was collected and dried in a vacuum desiccator over night to provide dry **NPDI_{hex}Br** (460 mg, 71%) as a dark red powder. **MALDI**: Theoretical: M⁺ 705.22 Found: 705.2185. **¹H NMR**: (500 MHz, CDCl₃) δ 8.92 (s, 2H, PDI Aryl), 8.88 (d, J = 8.0 Hz, 2H, PDI Aryl), 8.80 (br-d, J = 8.0 hz, 2H, PDI Aryl), 5.29 – 5.18 (m, 2H), 4.91 (t, J = 7.1 Hz, 2H), 3.36 (t, J = 6.7 Hz, 2H, CH₂-Br), 2.43 – 2.31 (m, 4H), 2.24 (dt, J = 14.7, 7.2 Hz, 2H), 2.07 – 1.96 (m, 4H), 1.86 – 1.79 (m, 2H), 1.56 – 1.43 (m, 4H), 0.99 (t, J = 7.5 Hz, 12H). **¹³C NMR**: (126 MHz, CDCl₃) δ 134.21, 132.14, 124.12, 123.36, 121.29, 119.01, 57.22, 46.19, 32.84, 31.84, 30.78, 27.17, 25.83, 24.67, 10.92.

NPDI_{hex}N₃ (3): To a 100 mL round bottom flask with a stir bar was added **NPDI_{hex}Br** (400 mg, 0.56 mmol), sodium azide (70 mg, 1.1 mmol) and DMF (20 mL). The reaction was capped with a septum and stirred at room temperature for 3 h. When TLC indicated complete consumption of the **NPDI_{hex}Br** the reaction mixture was diluted to 100 mL with Methanol and 10 mL of water was added to ensure the product had fully precipitated. The reaction mixture was filtered to give **NPDI_{hex}N₃** as a bright red solid (372 mg, 89%). No further purification was necessary. **MALDI**: Theoretical: M⁺ 668.31 Found: 668.3098. **¹H NMR**: (500 MHz, CDCl₃) δ 8.95 (s, 2H, PDI Aryl), 8.93 (d, J = 8.0 Hz, 2H, PDI Aryl), 8.83 (s, 2H, PDI Aryl), 5.23 (s, 2H), 4.92 (t, J = 7.1 Hz, 2H), 3.24 (t, J = 6.7 Hz, 2H, CH₂N₃), 2.42 – 2.31 (m, 4H), 2.25 (s, 2H), 2.01 (tt, J = 14.7, 7.4 Hz, 4H), 1.53 – 1.43 (m, 4H), 0.99 (t, J = 7.5 Hz, 12H). **¹³C NMR**: (126 MHz, CDCl₃) δ 134.28, 132.22, 124.18, 123.42, 121.37, 119.10, 57.21, 50.61, 46.22, 30.85, 28.08, 26.23, 25.83, 24.67, 10.91.

NPDI_{hex}PTZ (4): To a 10-20 mL microwave vial with a stir bar was added **NPDI_{hex}N₃** (100 mg, 0.15 mmol), **PTZ_{ac}** (38 mg, 0.16 mmol), copper sulfate (4 mg, 0.015 mmol), and sodium ascorbate (10 mmol 0.05 mmol). The vial was capped and purged with nitrogen for 10 min. 10 mL of a previously degassed 7:3 mixture of THF:water was cannula transferred to the reaction vial before heating to 60 °C for 18h. After TLC indicated complete consumption of the PDI starting material, the reaction was diluted with 50 mL CH₂Cl₂ and washed with water, dried with brine and magnesium sulfate, filtered through silica and the solvent was removed on a rotatory evaporator. The oily product was re-dissolved in CH₂Cl₂ and filtered through silica. Impurities were eluted with CH₂Cl₂ and the product eluted with EtOAc. The resulting solution was slurried with silica and alumina for 45 minutes before filtering through alumina. The solvent was removed on a rotatory evaporator and filtered with methanol to give **NPDI_{hex}PTZ** as a dark red solid (108 mg, 80%). **MALDI:** Theoretical: M + Na⁺ 928.36 Found: 928.3619. **CHN:** Theoretical: % C: 72.90, H: 5.67, N: 10.82. Found: % C: 72.51, H: 5.49, N: 10.51. **¹H NMR:** (500 MHz, CDCl₃) δ 9.02 (d, J = 8.0 Hz, 2H (PDI Aryl), 8.97 (s, J = 8.0 Hz, 2H, PDI Aryl), 8.88 (s, 2H, PDI Aryl), 7.25 (s, 2H, Triazole), 7.05 (dd, J = 7.6, 1.5 Hz, 2H, Ptz), 6.99 (ddd, J = 8.2, 7.5, 1.5 Hz, 2H, Ptz), 6.83 (td, J = 7.5, 1.1 Hz, 2H, Ptz), 6.72 (dd, J = 8.2, 0.8 Hz, 2H, Ptz), 5.26 – 5.18 (m, 2H, PDI imide), 5.16 (s, 2H, Ptz CH₂), 4.84 (t, J = 7.0 Hz, 2H, PDI CH₂), 4.22 (t, J = 7.1 Hz, 2H, Taz CH₂), 2.41 – 2.24 (m, 4H), 2.18 – 2.09 (m, 2H), 1.99 (qt, J = 11.0, 5.5 Hz, 4H), 1.82 – 1.74 (m, 2H), 1.41 (dt, J = 15.3, 7.6 Hz, 2H), 1.28 (dt, J = 15.1, 7.5 Hz, 2H), 0.97 (t, J = 7.5 Hz, 12H). **¹³C NMR:** (75 MHz, CDCl₃) δ 144.81, 144.22, 134.83, 132.82, 127.28, 127.13, 124.76, 124.04, 123.85, 122.75, 122.26, 119.69, 115.23, 57.79, 50.10, 44.90, 31.31, 29.93, 26.61, 26.00, 25.24, 11.49.

BrNPDI_{hex}N₃ (5): to a 100 mL round bottom flask with a stir bar was added **NPDI_{hex}N₃** (350 mg, 0.52 mmol), CH₂Cl₂ (25 mL) and liquid bromine (1 pipette, ~1.25 mL, large excess). The reaction

was capped with a septum and stirred at room temperature for 30 min. When TLC indicated complete consumption of **NPDI_{hex}N₃** the reaction mixture was quenched with saturated aqueous sodium bisulfite. The reaction mixture was then extracted with 2 times 50 mL saturated aqueous sodium bisulfite followed by drying with 2 times 50 mL brine. The organic phase was dried with magnesium sulfate and filtered through silica. The solvent was removed on a rotary evaporator. The product was dissolved in a minimum amount of CH₂Cl₂ and 50 mL MeOH was added. The CH₂Cl₂ was removed on a rotary evaporator. The suspended solid was filtered to give **BrNPDI_{hex}N₃** as a dark red solid (365 mg, 93%). No further purification was necessary. **MALDI**: Theoretical: M+H⁺ 745.21 Found: 745.2165. **¹H NMR**: (500 MHz, CDCl₃) δ 9.90 (s, 2H, PDI Aryl), 9.00 (s, *J* = 8.1 Hz, 4H, PDI Aryl), 8.90 (d, *J* = 8.1 Hz, 2H, PDI Aryl), 5.28 – 5.16 (m, 2H, PDI Imide), 4.83 (t, *J* = 5.8 Hz, 2H, PDI CH₂), 3.23 (t, *J* = 6.7 Hz, 2H, CH₂N₃), 2.44 – 2.31 (m, 4H), 2.21 (s, 2H), 2.05 (td, *J* = 13.7, 6.8 Hz, 4H), 1.56 (dd, *J* = 12.2, 4.0 Hz, 4H), 1.00 (p, *J* = 7.6 Hz, 12H). **¹³C NMR**: (126 MHz, CDCl₃) δ 133.76, 133.54, 131.56, 129.63, 126.80, 123.48, 122.88, 122.53, 121.36, 120.76, 118.03, 117.60, 76.71, 76.45, 76.20, 57.50, 57.35, 50.59, 46.08, 30.69, 28.05, 26.21, 25.79, 24.64, 24.58, 11.01, 10.97.

BrNPDI_{hex}PTZ (6): To a 10-20 mL microwave vial with a stir bar was added **BrNPDI_{hex}N₃** (225 mg, 0.3 mmol), **PTZ_{ac}** (71 mg, 0.3 mmol), copper sulfate (8 mg, 0.03 mmol) and sodium ascorbate (14 mg, 0.06 mmol). The vial was capped, and the headspace purged with nitrogen for 15 min. To the vial was added 20 mL of a previously degassed mixture of 7:3 THF: H₂O. The reaction was heated to 60 °C for 2 hours. When TLC indicated complete consumption of the starting material, the reaction was diluted to 50 mL with CH₂Cl₂ and extracted with CH₂Cl₂ and brine. The organic phase was dried with brine and filtered. The solvent was removed on rotary evaporator to give crude **BrNPDI_{hex}PTZ**. The product was purified by taking up in CH₂Cl₂ and

filtering through silica. CH₂Cl₂ was passed through silica until it ran clean, leaving the product as a red band at the top of the silica plug. CH₂Cl₂ with 10% methanol was passed through the silica to isolate **BrNPDI_{hex}PTZ**. The solvent was removed on a rotatory evaporator and the resulting red solid was filtered from methanol (216 mg, 73%). **MALDI**: Theoretical: M⁺ 983.28 Found: 983.2928. **¹H NMR**: (500 MHz, CDCl₃) δ 10.14 (d, *J* = 8.3 Hz, 1H, PDI Aryl), 9.02 (s, 1H, PDI Aryl), 8.95 (s, 2H, PDI Aryl), 8.84 (d, *J* = 7.2 Hz, 1H, PDI Aryl), 7.26 – 7.25 (m, 1H, Taz Aryl), 7.04 (dt, *J* = 5.0, 2.5 Hz, 2H, Ptz Aryl), 7.02 – 6.96 (m, 2H, Ptz Aryl), 6.86 – 6.80 (m, 2H, Ptz Aryl), 6.72 (dd, *J* = 8.2, 0.9 Hz, 2H, Ptz Aryl), 5.26 – 5.17 (m, 2H, PDI Imide), 5.16 (s, 2H, Ptz CH₂), 4.86 (t, *J* = 7.1 Hz, 2H, PDI CH₂), 4.21 (dt, *J* = 14.2, 7.1 Hz, 2H, Taz CH₂), 2.43 – 2.28 (m, 4H), 2.17 – 2.08 (m, 2H), 2.08 – 1.97 (m, 4H), 1.83 – 1.75 (m, 2H), 1.40 (dt, *J* = 10.7, 7.6 Hz, 2H), 1.27 (dt, *J* = 9.7, 7.7 Hz, 2H), 1.05 – 0.95 (m, 12H). **¹³C NMR**: (126 MHz, CDCl₃) δ 144.24, 143.64, 133.97, 133.76, 127.16, 126.70, 126.56, 123.72, 123.28, 122.74, 122.17, 121.68, 121.03, 118.40, 117.95, 114.65, 76.71, 76.45, 76.20, 57.47, 57.32, 49.51, 46.00, 44.31, 30.63, 29.33, 26.03, 25.41, 24.65, 24.59, 10.95, 10.91.

Bu₃SnNPDI_{hex} (8): To a 10-20 mL microwave vial with a stir bar was added **BrNPDI_{hex}** (800 mg, 1.13 mmol) and SiliaCat[®] DPP-Pd (440 mg, 0.13 mmol Pd). The reaction vial was brought into a glovebox where hexabutylstannane (0.8 mL, 800 mg, 1.24 mmol) was added. The vial was capped and removed from the box where 20 mL of previously degassed toluene was added. The reaction was heated to 100 °C with stirring for 1 hour. When TLC indicated complete consumption of **BrNPDI_{hex}**, the reaction was filtered through a silica plug with hexanes to remove residual hexabutylstannane, 2:1 CH₂Cl₂: hexanes to collect the desired product and acetone to recover the dimerized product. The solvent was removed on a rotatory evaporator to give **Bu₃SnNPDI_{hex}**

as a dark red viscous oil (630 mg, 0.069 mmol, 63%). This material was used “as-is” without further purification.

NPDI_{hex2}PTZ (9): Via Stille: To a 5-10 mL microwave vial with a stir bar was added **BrNPDI_{hex}PTZ** (107 mg, 0.11 mmol). The vial was then brought into a glove box where Pd(PPh₃)₄ (15 mg, 0.012 mmol) was added. The vial was capped and removed from the glove box. To the vial was added 1.5 mL of a 100 mg/mL solution of crude **Bu₃SnNPDI_{hex}** (~150 mg, 0.16 mmol) and 9 mL previously dried and degassed toluene. The reaction mixture was sparged with N₂ for 25 min before the reaction was heated in a microwave to 180 °C for 2h. TLC determined the complete consumption of **Bu₃SnNPDI_{hex}**. The reaction mixture was filtered through a silica plug to remove the catalyst. The solvent was removed on a rotatory evaporator to give a crude **NPDI_{hex2}PTZ**. The product was purified via column chromatography with CH₂Cl₂ with 2% methanol as eluent to give **NPDI_{hex2}PTZ** (75.3 mg, 0.049 mmol, 45%) as a dark red powder. This method of purification was unable to separate the desired product from a small amount of residual **PDI-C₆PTZ**.

NPDI_{hex2}PTZ (9): Via Negishi: To a 5-10 mL microwave vial with a stir bar was added **BrNPDI_{hex}PTZ** (50 mg, 0.05 mmol), **BrNPDI_{hex}** (36 mg, 0.05 mmol), and zinc (32 mg, 0.49 mmol). The vial was brought into a glove box where Pd₂DBA₃ (30 mg, 0.036 mmol) was added. The vial was capped and removed from the glove box. To the vial was added dry, degassed DMF (10 mL) before the reaction vial was sparged with N₂ for 10 min. The reaction was heated to 100 °C with stirring for 75 min. When TLC (40% EtOAc in toluene as eluent) showed complete consumption of the starting materials, the reaction mixture was filtered through a silica plug with CH₂Cl₂. The solvent was removed on a rotatory evaporator to yield the crude product. The product was purified via column chromatography with a toluene to EtOAc gradient, holding at 40% EtOAc until the desired product band was completely removed. Evaporation of the solvent on a rotatory

evaporator, followed by isolation with methanol yielded **NPDI_{hex2}PTZ** as a dark red solid (29 mg, 0.019 mmol, 38%). **CHN**: Theoretical: % C: 74.49, H: 5.92, N: 9.14. Found: % C: 74.21, H: 5.91, N: 9.04. **¹H NMR**: (500 MHz, CDCl₃) δ 9.28 (s, 1H, PDI Aryl), 9.23 (s, 1H, PDI Aryl), 9.10 (s, 1H, PDI Aryl), 9.05 (s, 1H, PDI Aryl), 8.89 (s, 2H, PDI Aryl), 7.97 (s, 2H, PDI Aryl), 7.71 (dd, J = 8.4, 2.2 Hz, 2H, PDI Aryl), 7.30 (d, J = 15.1 Hz, 1H, Taz), 7.09 (dd, J = 7.6, 1.4 Hz, 2H, Ptz Aryl), 7.04 (td, J = 8.2, 1.5 Hz, 2H, Ptz Aryl), 6.87 (td, J = 7.5, 1.0 Hz, 2H, Ptz Aryl), 6.77 (dd, J = 14.3, 6.8 Hz, 2H, Ptz Aryl), 5.21 (s, 4H, PDI Imide CH, PTZ-CH₂), 5.01 (two triplets, J = 24.1, 7.1 Hz, 6H, PDI Imide CH, 2x PDI CH₂), 4.29 (t, J = 7.0 Hz, 2H, Taz CH₂), 2.46 – 2.29 (m, 6H), 2.28 – 2.12 (m, 6H), 2.07 – 1.94 (m, 4H), 1.93 – 1.77 (m, 6H), 1.60 – 1.50 (m, 4H), 1.50 – 1.42 (m, 2H), 1.42 – 1.33 (m, 4H), 1.08 – 0.97 (m, 12H), 0.92 (dd, J = 14.9, 7.7 Hz, 3H), 0.83 (s, 11H). **¹³C NMR**: (126 MHz, CDCl₃) δ 144.30, 143.69, 140.41, 140.23, 134.69, 134.61, 134.47, 134.38, 132.35, 132.29, 129.84, 129.79, 126.75, 126.60, 126.33, 126.23, 124.39, 124.14, 123.31, 123.00, 122.21, 122.17, 121.74, 119.55, 119.52, 119.28, 119.25, 114.70, 76.71, 76.45, 76.20, 57.45, 57.04, 49.58, 46.57, 46.23, 44.37, 31.12, 30.89, 29.40, 26.44, 26.15, 25.51, 24.61, 24.46, 21.97, 13.46, 10.97, 10.69.

NPDI_{hex2}PTZ₂ (10): To a 10-20 mL microwave vial with a stir bar was added **BrNPDI_{hex}PTZ** (125 mg, 0.13 mmol) and zinc dust (42 mg, 0.66 mmol). The vial was brought into a glove box where Pd₂DBA₃ (20 mg, 0.02 mmol) was added. The vial was capped and removed from the glove box where 5 mL previously degassed DMF was added via cannula. The reaction was heated to 100 °C in a bead bath with stirring for 2.5 h when the solution had turned a dark blue. When TLC indicated complete consumption of starting material, the reaction was diluted to 75 mL with CH₂Cl₂ and an additional 10 mL of methanol was added. The resulting solution was filtered through silica to remove most of the palladium catalyst and zinc. The solvent was removed on a

rotatory evaporator. The resulting solid was redissolved in CH_2Cl_2 and filtered through silica again to remove any remaining traces of catalyst and zinc. The crude product was purified by column chromatography with a hexanes to EtOAc gradient. Combined fractions were slurried with celite and alumina before filtering from alumina to remove all metal contamination and neutralize acidic sites. Solvent was removed on a rotatory evaporator and **NPDI_{hex2}PTZ₂** was isolated as a fine red powder (75 mg, 66%). **MALDI:** Theoretical: $\text{M} + \text{Na}^+$ 1831.72 Found: 1831.59. **CHN:** Theoretical: % C: 72.99, H: 5.57, N: 10.83. Found: % C: 72.05, H: 5.43, N: 10.65. **¹H NMR:** (300 MHz, CDCl_3) δ 9.25 (s, 2H, PDI Aryl), 9.07 (s, 2H, PDI Aryl), 8.90 (s, 2H, PDI Aryl), 7.98 (d, $J = 8.1$ Hz, 2H, PDI Aryl), 7.73 (d, $J = 8.3$ Hz, 2H, PDI Aryl), 7.33 (s, 2H, Taz), 7.07 (m, 8H, Ptz Aryl), 6.95 – 6.84 (m, 4H, Ptz Aryl), 6.78 (d, $J = 8.1$ Hz, 4H, Ptz Aryl), 5.22 (s, 6H, Ptz- CH_2 , PDI Imide CH), 5.00 (t, $J = 6.8$ Hz, 6H, PDI Imide CH, PDI- CH_2), 4.31 (t, $J = 7.0$ Hz, 4H, Taz- CH_2), 2.36 (s, 4H), 2.26 (m, 8H), 2.09 – 1.95 (m, 4H), 1.89 (m, 8H), 1.53 (m, 4H), 1.44 – 1.32 (m, 4H), 1.02 (t, $J = 7.3$ Hz, 12H), 0.83 (br s, 12H). **¹³C NMR:** (75 MHz, CDCl_3) δ 144.88, 144.88, 144.27, 144.27, 134.97, 127.33, 127.33, 127.18, 127.18, 123.89, 123.89, 122.79, 122.79, 122.32, 122.32, 115.28, 115.28, 50.16, 50.16, 44.94, 44.94, 33.04, 31.46, 29.97, 29.97, 26.73, 26.08, 25.03, 11.27, 11.27.

ASSOCIATED CONTENT

Supporting Information: Materials and Methods, ¹H and ¹³C NMR spectra, MALDI spectra, EA results and supplementary figures (NMR, Full CV analysis, and UV-vis/PL spectra) are available free of charge via the Internet

AUTHOR INFORMATION

Corresponding Author

* Gregory C. Welch.

ACKNOWLEDGMENT

GCW acknowledges NSERC DG (435715-2013), CFI JELF (34102), CRC, and the U of C. JRC acknowledges the Province of Alberta as well as the U of C Faculty of Graduate Studies for graduate scholarships

Key Words: Organic Dyes, Perylene Diimide, N-Annulation, Phenothiazine, Molecular Dyads and Triads

REFERENCES

- [1] M. Hissler, A. Harriman, A. Khatyr, R. Ziessel, *Chem. – Eur. J.* **1999**, *5*, 3366–3381.
- [2] T. van der Boom, R. T. Hayes, Y. Zhao, P. J. Bushard, E. A. Weiss, M. R. Wasielewski, *J. Am. Chem. Soc.* **2002**, *124*, 9582–9590.
- [3] J. L. Logsdon, P. E. Hartnett, J. N. Nelson, M. A. Harris, T. J. Marks, M. R. Wasielewski, *ACS Appl. Mater. Interfaces* **2017**, *9*, 33493–33503.
- [4] A. Coskun, E. U. Akkaya, *J. Am. Chem. Soc.* **2005**, *127*, 10464–10465.
- [5] S. Amriou, A. Mehta, M. R. Bryce, *J. Mater. Chem.* **2005**, *15*, 1232–1234.
- [6] Y. Kunugi, K. Takimiya, N. Negishi, T. Otsubo, Y. Aso, *J. Mater. Chem.* **2004**, *14*, 2840–2841.
- [7] X. Kong, H. Gong, P. Liu, W. Yao, Z. Liu, G. Wang, S. Zhang, Z. He, *New J. Chem.* **2018**, 3211–3221.
- [8] D. Rolland, J. C. Brauer, L. Hartmann, L. Biniek, M. Brinkmann, N. Banerji, H. Frauenrath, *J. Mater. Chem. C* **2017**, *5*, 1383–1393.
- [9] K. Narayanaswamy, A. Venkateswararao, P. Nagarjuna, S. Bishnoi, V. Gupta, S. Chand, S. P. Singh, *Angew. Chem.* **2016**, *128*, 12522–12525.
- [10] A. Labrunie, J. Gorenflot, M. Babics, O. Alevéque, S. Dabos-Seignon, A. H. Balawi, Z. Kan, M. Wohlfahrt, E. Levillain, P. Hudhomme, et al., *Chem. Mater.* **2018**, 3474–3485.
- [11] J. Roncali, *Adv. Energy Mater.* **2011**, *1*, 147–160.
- [12] H. Kotani, K. Ohkubo, Y. Takai, S. Fukuzumi, *J. Phys. Chem. B* **2006**, *110*, 24047–24053.
- [13] F. D'Souza, O. Ito, *Chem. Commun.* **2009**, *0*, 4913–4928.
- [14] W. Chen, Q. Zhang, *J. Mater. Chem. C* **2017**, *5*, 1275–1302.
- [15] Y. Duan, X. Xu, Y. Li, Q. Peng, *Chin. Chem. Lett.* **2017**, *28*, 2105–2115.
- [16] W. Jiang, Y. Li, Z. Wang, *Acc. Chem. Res.* **2014**, *47*, 3135–3147.
- [17] C. Huang, S. Barlow, S. R. Marder, *J. Org. Chem.* **2011**, *76*, 2386–2407.
- [18] Z. Liu, Y. Wu, Q. Zhang, X. Gao, *J. Mater. Chem. A* **2016**, *4*, 17604–17622.
- [19] H. Langhals, A. J. Esterbauer, A. Walter, E. Riedle, I. Pugliesi, *J. Am. Chem. Soc.* **2010**, *132*, 16777–16782.

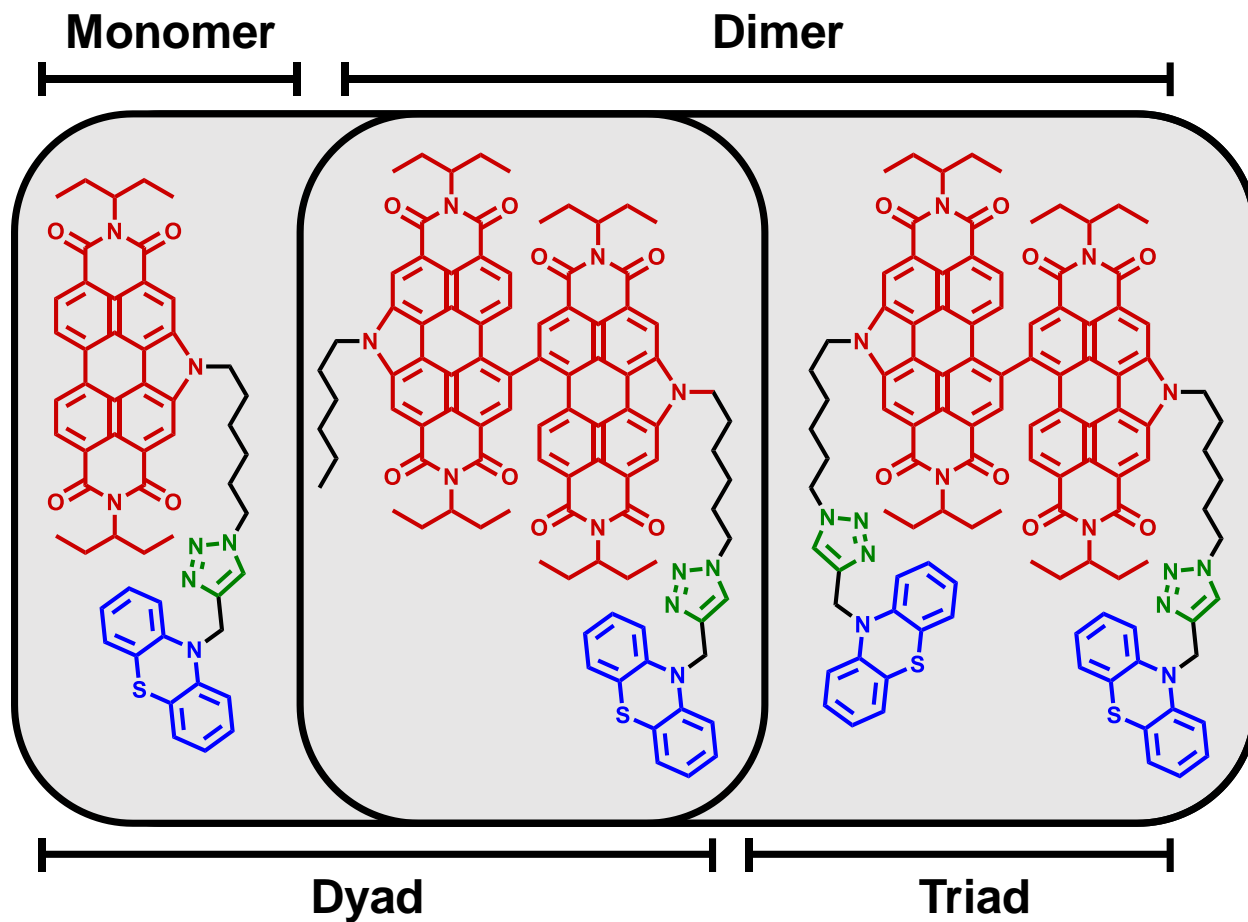
- [20] A. S. Lukas, Y. Zhao, S. E. Miller, M. R. Wasielewski, *J. Phys. Chem. B* **2002**, *106*, 1299–1306.
- [21] S. Fukuzumi, K. Ohkubo, J. Ortiz, A. M. Gutiérrez, F. Fernández-Lázaro, Á. Sastre-Santos, *Chem. Commun.* **2005**, *0*, 3814–3816.
- [22] S. Prathapan, S. I. Yang, J. Seth, M. A. Miller, D. F. Bocian, D. Holten, J. S. Lindsey, *J. Phys. Chem. B* **2001**, *105*, 8237–8248.
- [23] K. E. Brown, B. S. Veldkamp, D. T. Co, M. R. Wasielewski, *J. Phys. Chem. Lett.* **2012**, *3*, 2362–2366.
- [24] M. T. Vagnini, A. L. Smeigh, J. D. Blakemore, S. W. Eaton, N. D. Schley, F. D'Souza, R. H. Crabtree, G. W. Brudvig, D. T. Co, M. R. Wasielewski, *Proc. Natl. Acad. Sci.* **2012**, *109*, 15651–15656.
- [25] S. Leroy-Lhez, J. Baffreau, L. Perrin, E. Levillain, M. Allain, M.-J. Blesa, P. Hudhomme, *J. Org. Chem.* **2005**, *70*, 6313–6320.
- [26] Y. Li, H. Zheng, Y. Li, S. Wang, Z. Wu, P. Liu, Z. Gao, H. Liu, D. Zhu, *J. Org. Chem.* **2007**, *72*, 2878–2885.
- [27] L. Bu, X. Guo, B. Yu, Y. Qu, Z. Xie, D. Yan, Y. Geng, F. Wang, *J. Am. Chem. Soc.* **2009**, *131*, 13242–13243.
- [28] W.-S. Li, A. Saeki, Y. Yamamoto, T. Fukushima, S. Seki, N. Ishii, K. Kato, M. Takata, T. Aida, *Chem. – Asian J.* **2010**, *5*, 1566–1572.
- [29] S. Fukuzumi, K. Ohkubo, J. Ortiz, A. M. Gutiérrez, F. Fernández-Lázaro, Á. Sastre-Santos, *J. Phys. Chem. A* **2008**, *112*, 10744–10752.
- [30] J. Baffreau, S. Leroy-Lhez, N. Văn Anh, R. M. Williams, P. Hudhomme, *Chem. – Eur. J.* **2008**, *14*, 4974–4992.
- [31] K. Qvortrup, M. Å. Petersen, T. Hassenkam, M. B. Nielsen, *Tetrahedron Lett.* **2009**, *50*, 5613–5616.
- [32] J. E. Bullock, R. Carmieli, S. M. Mickley, J. Vura-Weis, M. R. Wasielewski, *J. Am. Chem. Soc.* **2009**, *131*, 11919–11929.
- [33] W. Tan, X. Li, J. Zhang, H. Tian, *Dyes Pigments* **2011**, *89*, 260–265.
- [34] Y. Wu, Y. Zhen, Z. Wang, H. Fu, *J. Phys. Chem. A* **2013**, *117*, 1712–1720.
- [35] H. Langhals, S. Kirner, *Eur. J. Org. Chem.* **1999**, *2000*, 365–380.
- [36] A. D. Hendsbee, J.-P. Sun, W. K. Law, H. Yan, I. G. Hill, D. M. Spasyuk, G. C. Welch, *Chem. Mater.* **2016**, *28*, 7098–7109.
- [37] S. M. McAfee, S. V. Dayneko, P. Josse, P. Blanchard, C. Cabanetos, G. C. Welch, *Chem. Mater.* **2017**, *29*, 1309–1314.
- [38] Z. Ma, H. Fu, D. Meng, W. Jiang, Y. Sun, Z. Wang, *Chem. – Asian J.* **2018**, *13*, 918–923.
- [39] R. K. Gupta, D. S. Shankar Rao, S. K. Prasad, A. S. Achalkumar, *Chem. – Eur. J.* **2018**, *24*, 3566–3575.
- [40] M. Vespa, J. R. Cann, S. V. Dayneko, O. A. Melville, A. D. Hendsbee, Y. Zou, B. H. Lessard, G. C. Welch, *Eur. J. Org. Chem.* **2018**, *2018*, 4592–4599.
- [41] A. D. Hendsbee, S. V. Dayneko, J. A. Pells, J. R. Cann, G. C. Welch, *Sustain. Energy Fuels* **2017**, *1*, 1137–1147.
- [42] Y. Iida, *Bull. Chem. Soc. Jpn.* **1971**, *44*, 663–667.
- [43] A. P. Kaur, N. E. Holubowitch, S. Ergun, C. F. Elliott, S. A. Odom, *Energy Technol.* **2015**, *3*, 476–480.
- [44] V. A. Chiykowski, B. Lam, C. Du, C. P. Berlinguette, *Chem. Commun.* **2017**, *53*, 2367–2370.

- [45] D. Meng, D. Sun, C. Zhong, T. Liu, B. Fan, L. Huo, Y. Li, W. Jiang, H. Choi, T. Kim, et al., *J. Am. Chem. Soc.* **2016**, *138*, 375–380.
- [46] D. Sun, D. Meng, Y. Cai, B. Fan, Y. Li, W. Jiang, L. Huo, Y. Sun, Z. Wang, *J. Am. Chem. Soc.* **2015**, *137*, 11156–11162.
- [47] C. Sae-Lim, D. J. Sandman, B. M. Foxman, M. Sukwattanasinitt, *J. Macromol. Sci. Part A* **2006**, *43*, 1929–1936.
- [48] S. Dey, A. Efimov, H. Lemmetyinen, *Eur. J. Org. Chem.* **2011**, *2011*, 5955–5958.
- [49] Y. Duan, X. Xu, H. Yan, W. Wu, Z. Li, Q. Peng, *Adv. Mater.* **2017**, *29*, 1605115.
- [50] J. Cann, S. Dayneko, J.-P. Sun, A. D. Hendsbee, I. G. Hill, G. C. Welch, *J. Mater. Chem. C* **2017**, *5*, 2074–2083.
- [51] J. R. Cann, C. Cabanetos, G. C. Welch, *ChemPlusChem* **2017**, *82*, 1359–1364.
- [52] C. Kaufmann, D. Bialas, M. Stolte, F. Würthner, *J. Am. Chem. Soc.* **2018**, *140*, 9986–9995.
- [53] F. Würthner, *Chem. Commun.* **2004**, 1564–1579.
- [54] L. Zhang, D. He, Y. Liu, K. Wang, Z. Guo, J. Lin, H.-J. Zhang, *Org. Lett.* **2016**, *18*, 5908–5911.
- [55] S. Dayneko, A. Hendsbee, G. Welch, *Small Methods* **2018**, *2*, 1800081.

TOC Text

Synthesis of monomeric and dimeric perylene diimide dyads and triads via N-annulation at the bay position

TOC Graphic



Accepted Manuscript